Chemistry–A European Journal
Research Article
doi.org/10.1002/chem.202201084
Chemistry Europe
European Chemical Societies Publishing
www.chemeurj.org

Spectroscopic, Crystallographic, and Electrochemical Study of Different Manganese(II)-Substituted Keggin-Type Phosphomolybdates

Jan-Christian Raabe,[a] Jakob Albert,[a] and Maximilian J. Poller*[a]

Abstract: Adjusting the RedOx activity of polyoxometalate catalysts is a key challenge for the catalysis of selective oxidation reactions. For this purpose, the possibility of influencing the RedOx potential by the introduction of an additional RedOx-active element was investigated. Thereby, Keggin-type polyoxometalates (POMs) with up to three different elements in the metal framework were created. An advanced and reproducible synthetic procedure to incorporate Mn^{II} and additionally V^{V} into Keggin-type heteropolyacids alongside comprehensive characterization of the new molecules is presented. The success of our syntheses was confirmed by vibrational spectroscopy (IR and Raman) and elemental analysis. Furthermore, the new compounds were analyzed by NMR spectroscopy to investigate the characteristics of the POMs in solution. The structures of successfully crystalized compounds were determined by single-crystal X-ray diffraction. Moreover, all synthesized compounds were characterized using UV/Vis spectroscopy and electrochemical analysis to get further insights into the electronic transfer processes and redox potentials.

Introduction

Polyoxometalates (POMs) have been the focus of intensive research for more than a century. Nevertheless, new applications for functional polyoxometalates are still being investigated and the synthesis of new, fit-for purpose derivatives of POMs remains a very active field of research.[1] Applications for POMs range from the medical field[2] to electronic devices[3,4] and to green catalysis.[5–7] For catalytic applications, Keggin-type POMs have been proven particularly useful. Their high Brønsted acidity makes them suitable catalysts for acid catalyzed reactions such as ester hydrolysis.[8] Additionally, by substituting the framework metal of Keggin-type POMs with a RedOx active transition metal,[9] they become excellent bifunctional RedOx and acid catalysts.[9,10] A prime example for this are vanadium substituted phosphomolybdates, specifically $H_8PV_5Mo_7O_{40}$ (HPA-5), which has been successfully applied as a catalyst for the conversion of biomass to formic acid[6,10] and for the oxidative desulfurization of fuels.[7]

To enable a broader range of RedOx catalytic applications, it is necessary to tune the RedOx potential of the POM to the desired application. Therefore, we have investigated the possibility of introducing an additional RedOx-active element with the goal of adjusting the RedOx potential of the POM. Thereby, we created Keggin-type POMs with up to three different elements in the metal framework.

In general, the introduction of RedOx active metals into the POM framework can be achieved either by the reaction of a metal precursor with a lacunary-POM, or by adding a suitable metal precursor in the desired stoichiometry during the initial self-assembly based synthesis of the POM. A lacunary type POM is a defect POM structure in which one or more MO_6 octahedrons are removed from the parent POM structure.[11,12] The defects can then be filled with suitable transition metal salts, resulting in substituted POMs. This method is limited to low substitution levels as the lacunary structure only allows filling up the number of vacancies (usually between 1 and 3).[11,12] In contrast, the self-assembly process, entails combining the various metal precursors in the desired stoichiometry, so that under reaction conditions the precursor compounds arrange themselves to form the final POM structure.[13] This method has been successfully employed for substitutions of up to half of the framework metals in the Keggin structure.[9] Since the introduction of additional elements generally benefits from an overall higher substitution, we employed this synthetic strategy.

The transition metal of choice for our investigation was manganese, which is known for versatile redox chemistry. Although the use of Mn(II) substituted bimetallic POMs has been reported previously,[14,15] no detailed synthetic procedure for higher Mn(II)-substituted POMs has been published and no detailed analytical characterization has been performed. The specific incorporation of Mn(II) into the $H_{(3+x)}[PV_xMo_{(12-x)}O_{40}]$ Keggin framework has not yet been described in the literature at all. In this work we present a synthetic procedure leading to the introduction of Mn(II) to form bimetallic (Mn(II), Mo(VI)) and

[a] J.-C. Raabe, Prof. Dr. J. Albert, Dr. M. J. Poller
Institute of Technical and Macromolecular Chemistry
Hamburg University
Bundesstrasse 45, 20146 Hamburg (Germany)
E-mail: maximilian.poller@chemie.uni-hamburg.de

Supporting information for this article is available on the WWW under https://doi.org/10.1002/chem.202201084

Table 1. Results from ICP-OES and TGA analysis of the different HPA–X-Y compounds.

Compound	Molecular composition	P/V/Mn/Mo ratio[a]	Hydration water[b] [mol/mol-POM]
HPA-0-1	$H_7[PMnMo_{11}O_{40}]$	1.14/0/1.07/11	8
HPA-0-2	$H_{11}[PMn_2Mo_{10}O_{40}]$	1.05/0/2.03/10	10
HPA-1-1	$H_8[PVMnMo_{10}O_{40}]$	1.26/1.03/1.05/10	8
HPA-1-2	$H_{12}[PVMn_2Mo_9O_{40}]$	1.24/1.05/2.09/9	10
HPA-3-2	$H_{14}[PV_3Mn_2Mo_7O_{40}]$	1.27/3.09/2.09/7	23
HPA-5-1	$H_{12}[PV_5MnMo_6O_{40}]$	1.29/5.21/1.04/6	23

HPA-*X*-*Y* is $H_{(3+x+4y)}[PV_xMn_yMo_{(12-x-y)}O_{40}]$. [a] The ratios P/V/Mn/Mo were determined by ICP-OES analysis. The data were normalized to the targeted Mo content. H_3PO_4 was used in a slight excess during the synthesis, therefore the high P content may be attributed to residual H_3PO_4. [b] The content of hydration water was determined by TGA analysis.

trimetallic (Mn(II), V(V), Mo(VI)) Keggin-type POMs. To the best of our knowledge, this is the first time that Keggin-type POMs with three different elements in the position of the framework metal (i.e. without considering the heteroatom position) have been synthesized and fully characterized. Additionally, we have performed comprehensive analytical characterization of the new compounds, including electrochemical investigations to determine the influence of Mn(II) on the redox activity of the POM.

Results and Discussion

To achieve the incorporation of Mn(II) into the Keggin structure we have used manganese(II) acetate $Mn(OAc)_2$ as suggested by Patel and Pathan[15] in an improved synthetic procedure based on the self-assembly synthesis of bimetallic V(V)-Mo(VI)-POMs described by Odyakov et al.[16–18] In contrast to the synthesis via lacunary structures, this procedure allows higher degrees of substitution and is less pH sensitive.

In our procedure, we first prepared a solution of MoO_3 and phosphoric acid, to which the V(V) precursor solution and later the $Mn(OAc)_2$ were added. The ratio of the metal precursors corresponds to the stoichiometry of the final product. During the synthesis of the Mn(II) substituted POMs, a clear, homogeneous, characteristically coloured reaction solution was formed. No precipitate was observed, therefore it can be assumed that no insoluble Mn(II) species such as manganese(II) oxide or phosphate was formed. Subsequently the solvent was removed under reduced pressure and elevated temperature to yield the final product. On the basis of this procedure, we have successfully synthesized bimetallic Keggin-type POMs with a ratio of Mn(II)/Mo(VI) of 1/11 and 2/10 as well as trimetallic Keggin-type POMs with different Mn(II)/V(V)/Mo(VI) ratios ranging from 1/1/10 to 1/5/6. Experiments attempting the incorporation of more than two Mn(II) ions did not yield a defined product. Attempts to incorporate Mn(VII) into the Keggin structure, using potassium permanganate as a precursor, did not lead to the desired compounds. Detailed synthetic procedures for all described compounds with the corresponding analytical data in Figures S1–S36 can be found in the Supporting Information.

To verify the successful incorporation of Mn(II) in the Keggin cluster, the targeted stoichiometry was confirmed using ICP-OES (Table 1). In addition, we determined the amount of hydration water using thermogravimetric analysis (TGA). The low-substituted POMs (up to 3 atoms) have crystal water contents between 8 and 10 water molecules per Keggin unit, whereby the highly-substituted POMs (5 and 6 atoms out of 12) have contents of 23 water molecules per POM molecule.

The integrity of the Keggin structure was shown by ATR-FTIR (Figure 1 and 2) and Raman spectroscopy (Figure 3 and 4), respectively. IR spectroscopy of Keggin-type POMs in general has already been discussed in literature to a great extent.[10,19,20] Therefore it is a well-established suitable method to confirm the structure type of the new compounds. The data of HPA-0-1 are consistent with those of Patel and Pathan.[15] No literature data exist for HPA-0-2 and the V(V)/Mn(II) substituted POMs, here only the comparison to the V(V) substituted POMs published in the literature can be made.[10] The FTIR spectra of the newly

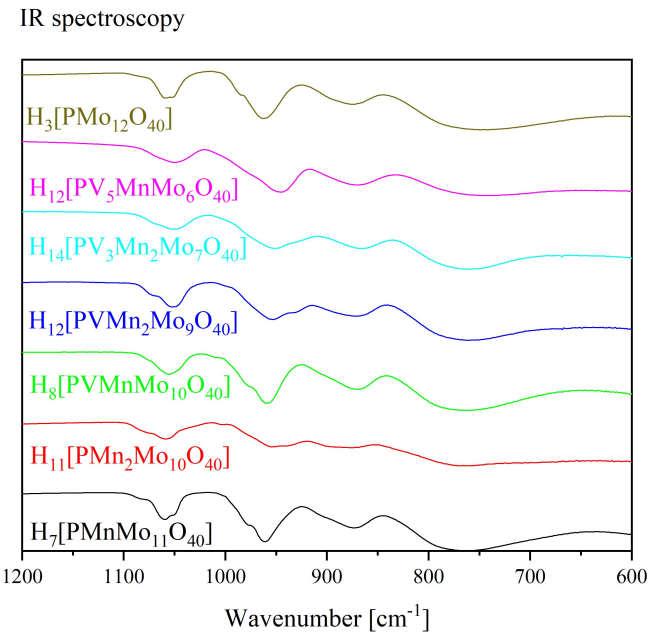

Figure 1. FTIR (ATR) spectra of the Mn^{II}-substituted HPA-X-Y POMs compared to $H_3[PMo_{12}O_{40}]$.

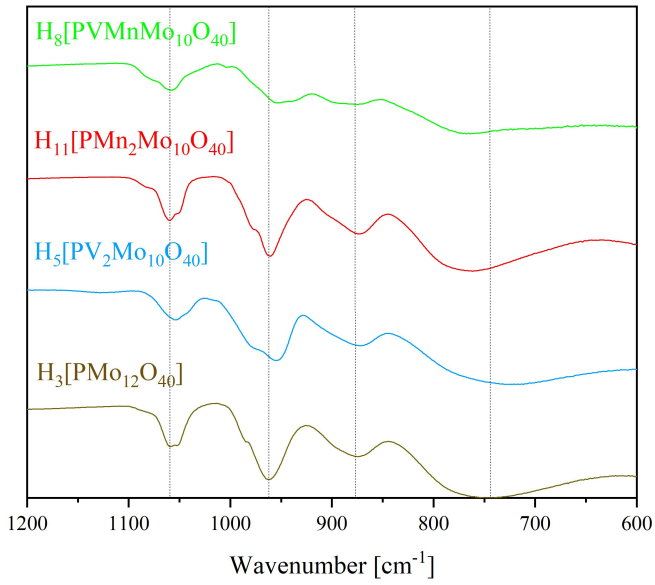

Figure 2. Superimposed IR spectra of the two-fold metal-substituted POMs HPA-1-1, HPA-0-2 and HPA-2-0, compared with the IR spectrum of HPA-0-0.

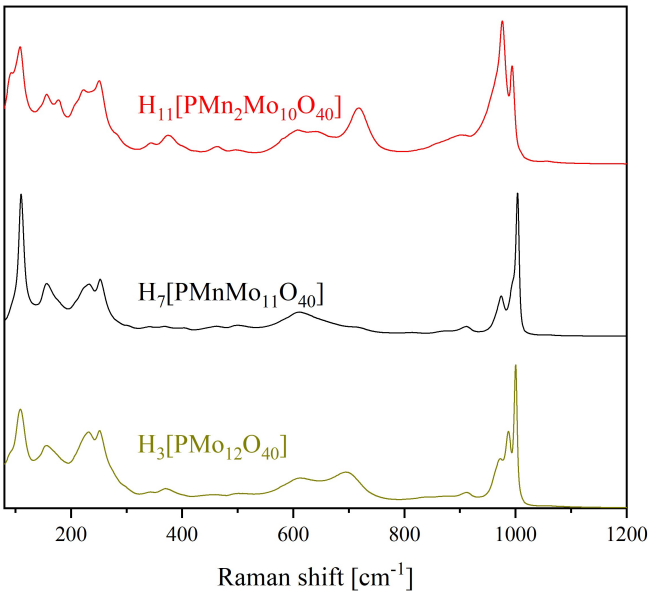

Figure 4. Superimposed Raman spectra of the only Mn^{II}-substituted POMs HPA-0-2, HPA-0-1 and in comparison with HPA-0-0.

Raman spectroscopy

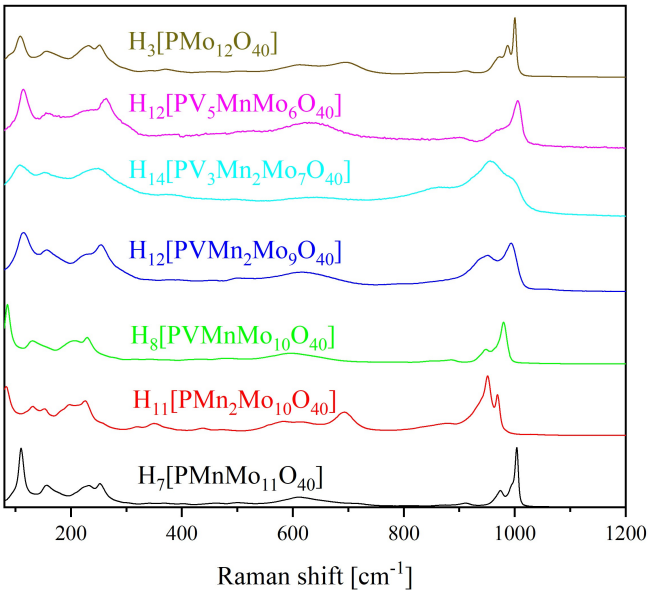

Figure 3. Raman spectra of the Mn^{II}-substituted HPA-X-Y POMs compared to $H_3[PMo_{12}O_{40}]$.[19]

synthesized POMs are shown in Figure 1 and 2, with spectra of $H_3[PMo_{12}O_{40}]$ (HPA-0-0) for comparison.

The IR spectrum of HPA-0-0 shows bands for P–O vibration at 1059 cm^{-1}, for the terminal M=O_t vibration at 962 cm^{-1}, and for the M–O–M vibrations at 877 cm^{-1} and 744 cm^{-1}, respectively. In comparison, the P–O, M=O_t and M–O-M bands of the substituted POMs are shifted to lower wavenumbers, indicating successful incorporation of the Mn(II) ions into the Keggin structure (Table 2). All spectra and more detailed tables can be found in the Supporting Information (Figure S43–S46 and Table 1–3 Supporting Information).

A closer look at the superimposed IR spectra of the two-fold substituted POMs (in Figure 2 with $H_5[PV_2Mo_{10}O_{40}]$ (HPA-2-0) as HPA-*X*-0 equivalent) reveals that the peaks of the two-metal substituted POMs are shifted to lower wavenumbers compared to HPA-0-0. This can possibly be explained by the fact that the Mo(VI) positions are occupied by metals with significantly smaller ionic mass, so that the corresponding oscillation modes can be excited more easily. The appearance of a shoulder in the P–O-stretching has previously been reported as an indicator for substitution in Keggin structures.[19] This is caused by substitution of the scaffolding metal (in our case Mo) with an element of significantly lower mass (Mn and V) and is therefore a strong indicator for the successful incorporation of a transition metal into the Keggin-type phosphomolybdate. Additionally, the main

Table 2. Position of the characteristic vibration bands for HPA-X-Y POMs in the IR spectrum.

Vibration type ν_{as}	HPA-0-0	HPA-0-1	HPA-0-2	HPA-1-1	HPA-1-2	HPA-3-2	HPA-5-1
(P=O)	1059	1060	1059	1055	1053	1052	1049
(M=O_t)	962	961	954	959	953	951	945
(M–O–M)$_{vertex}$	877	874	874	871	869	866	870
(M–O–M)$_{edge}$	744	762	767	762	757	759	743

Table 3. Overview of selected bond lengths (mean value) versus the sum of covalent radii of the elements involved.[30]

	P_1–O_1	O_1–M_1	M_1–$O_{2,3}$	M_1=O_4
Found bond length (mean value) [Å]	1.538	2.422	1.884	1.658
Sum of covalent radii[30] [Å]	1.74	2.01 (O–Mo) 1.97 (O–V) 1.82 (O–Mn)		

peaks in some spectra show a shift to lower wavenumbers with increasing substitution. This is in essence the same phenomenon, however, the small difference in excitation energy is not resolved for these broad peaks. As a result, the observed effect is a small shift of the peak maximum instead of the formation of a shoulder in the peak (which might also cause a shift of the peak maximum). Table 3 in the Supporting Information shows the IR data of the Mn(II) substituted POMs compared with the corresponding literature IR data of the analogous $H_{(3+x)}[PV_xMo_{(12-x)}O_{40}]$ (HPA-*X*-0), in which the Mo(VI) position are only substituted by V(V).[10]

In conclusion, the IR spectra confirm the Keggin structure type and the successful incorporation of the lighter transition metals (Mn(II), V(V)) into the Keggin structure. It can be observed that the trend of peak shift with increasing V(V) substitution can also be observed for the Mn(II) substituted POMs.

The same can be concluded from the Raman spectra (Figure 3 and 4).[19,21] In particular, the Raman spectra of the substituted POMs (Figure 3 and 4) show very strong differences (especially in the range of the M=O_t vibration bands) compared to the unsubstituted HPA-0-0, suggesting successful incorporation of the transition metals into the Keggin structure (Figure 4).

Due to the incorporation of Mn(II) the M=O_t stretch band is shifted from 1001 cm^{-1} (HPA-0-0) to 1004 cm^{-1} (HPA-0-1). The M=O_t band at 987 cm^{-1} (HPA-0-0) vanishes within the M=O_t band at 1004 cm^{-1} in HPA-0-1 (resulting in a shoulder formation in HPA-0-1). The band at 1004 cm^{-1} in HPA-0-1 shifts to 994 cm^{-1} in HPA-0-2 and loses intensity, while the band at 975 cm^{-1} in HPA-0-1 becomes an intense, broad band at 977 cm^{-1} in HPA-0-2. The vibrational band in HPA-0-2 at 109 cm^{-1}, which can be assigned to an O–M–O vibration, becomes an additional shoulder at 93 cm^{-1} due to the two-fold Mn(II) substitution, which is not visible in the Raman spectra of HPA-0-1 and HPA-0-0 (Figure 4). The change of shape of the peaks in the Raman spectra (see also Figure S45 and S46 in the Supporting Information) are a result of the different ionic masses of the different transition metals. This can be seen as an indicator for successful incorporation of Mn(II) into the $[PMo_{12}O_{40}]^{3-}$ anion. Another advantage of Raman spectroscopy is that the range around 80 cm^{-1} to 400 cm^{-1} can be investigated, which was not possible with the available IR spectrometer. The Raman spectra (Figure 3, 4 and Figures S45 and S46 in the Supporting Information) show that the region below 400 cm^{-1} is relevant for interpretation because there are some M–O–M vibrational bands in this region. The peaks in the range 80 cm^{-1} to 300 cm^{-1} show mainly the different types of M–O–M vibrations. These peaks, as well as the M=O_t vibrations at 900 cm^{-1} to 1000 cm^{-1} are shifted and broadened with increasing V(V) and Mn(II) substitution. The cause for this is the same effect that has been discussed above for the formation of shoulders on the peaks. The P–O vibrational band is apparently not Raman active but can be seen in the IR spectra.

To elucidate correlations between structural features on the molecular level for performance in future catalytical applications, additional characterization by single-crystal X-ray diffraction (XRD) was carried out.[22–29] Although several crystal structures of Keggin-type POMs are known, there is little literature for single crystals of Keggin-POMs in their protonated form, most likely due to the difficulty in crystallizing them.[28,29] Nevertheless, we were able to successfully analyze single crystals of five out of the six new POMs presented in this paper. The crystals were obtained by slow evaporation of the solvent from an aqueous solution of the respective compound in a desiccator under reduced pressure.

Figure 5 shows the asymmetric unit of the POM HPA-1-1 with six atoms and the corresponding numbering of the atoms. Images of the other structures and tables of selected bond lengths can be found in the Supporting Information (Figures S47–S51), the full crystallographic information files (cif) are available through the CCDC database (deposition numbers: HPA-0-1: 2141261, HPA-0-2: 2141263, HPA-1-1: 2141259, HPA-1-2: 2141262, HPA-5-1: 2141260).

The asymmetric unit of the structures only contains one metal atom, indicating, that all twelve metal positions are

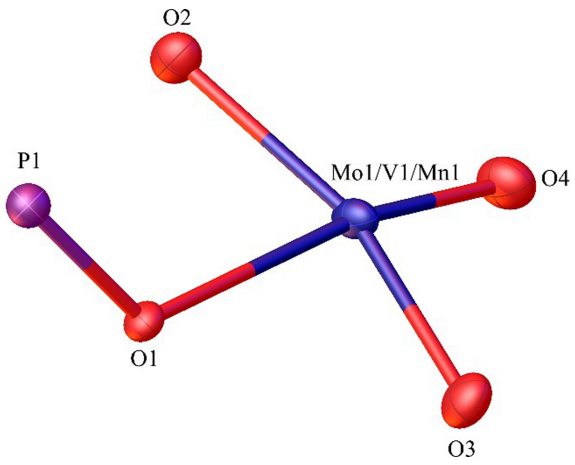

Figure 5. Asymmetric unit of a crystal of HPA-1-1 with the corresponding numbering of the atoms, hydrogen atoms have not been modeled. Purple: phosphorous, red: oxygen, and blue: metals (Mo, V, Mn).

equivalent. The incorporation of Mn(II) and V(V) becomes apparent, when comparing the refinement of the metal position with 12/12 occupancy Mo(VI) versus the metal ration determined by ICP-OES (e.g. 1/12 Mn(II), 1/12 V(V), 10/12 Mo(VI) for HPA-1-1), which results in a significantly better model (i.e. less residual negative electron density).

The crystal structures verify the Keggin structure type: the phosphorus atom as heteroatom in the center of the cluster is tetrahedrally coordinated by four oxygen atoms, while all metals are in distorted octahedral coordination surrounded by six oxygen atoms. All four oxygen atoms surrounding the central phosphorus atom are part of the four Mo_3O_{13} units. No other transition metal cations were identified outside the Keggin structure. Since H atoms do not have sufficient electron density to be located by XRD, they have been omitted in the refined model. Hydration water in the crystal lattice was strongly disordered and could not be modelled in most cases. Therefore, solvent mask (SQUEEZE) was applied to the residual voids and the electron density therein was assigned to hydration water, in order to obtain a better refinement.[27]

Most of the POMs crystallize in highly symmetric cubic space groups. The POMs HPA-0-1 and HPA-0-2 crystallize in the cubic space group Fd-3 (203), while the V(V) containing POMs HPA-1-1 and HPA-1-2 exist in the cubic space group Fd-3 m (227). This coincides with the presence of only one metal atom in the asymmetric unit. As a result, a discrete substitution pattern cannot be recognized. The lattice parameters *a*, *b* and *c* are on average 23 Å and the lattice angles α, β and γ are 90 °. Furthermore, it is noticeable that the POM with increased V(V) content HP-5-1 crystallizes in the trigonal space group R-3 (148), respectively. However, all metal elements are statistically distributed over all metal positions and therefore no discrete substitution pattern was recognized. For HPA-5-1, the lattice parameters *a* and *b* are 15.2 Å and *c* is 38.9 Å. The lattice angles α and β are 90 ° and γ 120 ° (Table 4 Supporting Information). It follows that the unit cells of the low-substituted POMs (up to 3 metals out of 12) are almost the same, while the unit cell of the high-substituted POMs (6 metals out of 12) is very different from those of the low-substituted POMs and, all in all, have a much smaller volume. Table 3 shows an overview of selected bond lengths (mean value of all found bond lengths of all HPA-*X*-*Y* POMs) versus the sum of covalent radii[30] of the elements involved:

The average bond length of the P-O bond is about 1.538 Å (P_1–O_1), while the average bond lengths of the oxygen-metal bonds connecting the metals to the central phosphorus atom is 2.422 Å (O_1–M_1). Assuming that the ideal bond lengths result from the sum of the covalent radii of the atoms involved, the length of the P–O bond (P: 111 pm; O: 63 pm) is 174 pm (1.74 Å).[30] Thus, the P–O bond of 1.538 Å is significantly shorter than the sum of the covalent radii, indicating double bond character. Furthermore, the average metal-oxygen-metal bond is 1.884 Å long (Bond M_1–$O_{2,3}$), while the average bond lengths of the terminal oxygen-metal bonds are 1.658 Å (M_1=O_4) (see Supporting Information Table 5). Accordingly, the bond lengths for the O–Mo bond (Mo: 138 pm) would be 201 pm (2.01 Å), for the O–V bond (V: 134 pm) 197 pm (1.97 Å) and for the O–Mn bond (Mn: 119 pm) 182 pm (1.82 Å).[30] Thus, the O–M bond of 1.884 Å is in the range between the O–V and O-Mn bond. When discussing the bond lengths, it is important to note that several metals and oxygen atoms are present in the asymmetric unit of the POM HPA-5-1 (Table 5 Supporting Information). Here, the metal-oxygen bonds are in the range between 1.798 Å and 2.044 Å, so that metal-oxygen bonds can be found that are in the range of O–Mn, O–V and O–Mo bond lengths. It is striking that the O_1–M_1 bond of 2.422 Å is significantly longer than all other bonds. The terminal M_1=O_4 bonds are significantly shorter with an average of 1.658 Å, which can be explained by the double bond character of the M_1=O_4 bond. Compared to the crystal structure of HPA-0-0, the following trend is noticeable: In HPA-0-0 the P–O bond is 1.534 Å, the O_1–M_1 bond is 2.439 Å, the M_1–$O_{2,3}$ bond is 1.916 Å and the M_1=O_4 bond is 1.674 Å.[31] It follows that the P–O bond length gets about 0.004 Å longer due to the substitution with the foreign metals V(V) and Mn(II), while the O_1–M_1 bond shortens by about 0.017 Å. The M_1–$O_{2,3}$ bond shortens about 0.032 Å. Likewise, the M_1=O_4 bond short-

Table 4. Weighted average of calculated bond lengths (sum of covalent radii) and observed bond lengths of each bond in each POM.

	Sum of covalent radii*/observed bond length [Å]			
	P_1–O_1	O_1–M_1	M_1–$O_{2,3}$	M_1=O_4
HPA-0-0	1.74/1.534	2.01/2.439	2.01/1.916	2.01/1.674
HPA-0-1	1.74/1.536	1.99/2.433	1.99/1.839	1.99/1.681
HPA-0-2	1.74/1.539	1.98/2.430	1.98/1.836	1.98/1.678
HPA-1-1	1.74/1.537	1.99/2.422	1.99/1.913	1.99/1.663
HPA-1-2	1.74/1.532	1.98/2.425	1.98/1.913	1.98/1.666
HPA-5-1	1.74/1.543	1.98/2.404	1.98/1.923	1.98/1.637

*$BL=\frac{a(r_O+r_{Mo})+b(r_O+r_V)+c(r_O+r_{Mn})}{a+b+c}$ with *BL* the weighted average bond length, r_x the covalent radii of the corresponding elements x and *a*, *b* and *c* the weighting factors (e.g. for HPA-1-1: $a=10$, $b=1$ and $c=1$).

Table 5. Chemical shifts obtained from ^{31}P and ^{51}V NMR spectra of the HPA–X-Y compounds in comparison with the ^{31}P NMR shifts of HPA-0-0.[10]

Compound	HPA-0-0	HPA-0-1	HPA-0-2	HPA-1-1	HPA-1-2	HPA-3-2	HPA-5-1
^{31}P NMR	−3.75	−2.96, −3.77	−2.88, −3.78	−4.04	−3.57, −3.99	Multiple signals −1.13 to −4.66	Multiple signals 0.09 to −4.95
^{51}V NMR	–	–	–	-532.1	−531.7, −538.8	Multiple signals −495.2 to −617.6	Multiple signals −508.7 to −608.1

ens by 0.016 Å.[31] The result is an overall contraction of the averaged MO_6 octahedra with metal substitution (Table 4). This also indicates the successful incorporation of metals with a smaller covalent/ionic radius (Mo = 138 pm, V = 134 pm, Mn = 119 pm).[30] Table 4 shows a comparison between the weighted sum of covalent radii (formula shown in Table 4) and the bond lengths found for each POM. So, a direct comparison between the expected and the found bond lengths is possible, indicating that the bond lengths vary depending on the substitution pattern.

As can be seen from the crystal structure data, the MO_6 octahedra are slightly distorted. In the following, the four bond angles of the O_4=M_1–$O_{2,3}$ bonds were measured, and the mean value formed in each case. For HPA-0-1 this angle is 101.86 °, for HPA-0-2 101.83 °, for HPA-1-1 101.734 °, for HPA-1-2 101.768 ° and for HPA-5-1 100.612 °. This shows that the octahedra are distorted compared to the ideal octahedron, in which the optimal O–M–O angle is 90 °.[32,33]

The distortion of the PO_4 tetrahedra in comparison with the ideal tetrahedron geometry was analyzed as follows: All three angles of the O_1-P_1-O_1 bonds were measured and the mean value was calculated. For HPA-0-1, HPA-0-2, HPA-1-1 and HPA-1-2, the angle is about 109.471 °. This means that the tetrahedral angles found are very close to the ideal value of 109.5 °.[34,35] This shows that the metal substitution in the Keggin framework has no significant influence on the P–O bonds, especially the O–P–O bond angle. For the high metal-substituted Keggin-type POM, the tetrahedral bond angle is 109.416 ° for HPA-5-1. This shows that the P–O bond and its bond angles are slightly affected by metal substitution when high degrees of substitution are obtained (six out of twelve metals in HPA-5-1).

Figure 6 shows the exemplary solid-state structure of HPA-1-1. According to the single crystal structure analysis, the compound crystallizes in the space group Fd-3 m (227). The cell parameters *a*, *b* and *c* are equal according to the cubic crystal system and are about 23 Å. The lattice angles are all 90 °. There are six atoms in the asymmetric unit: The central phosphorus atom, the internal oxygen atom, one of the twelve metal atoms, the metal-metal bridging oxygen and the terminal oxygen atom. In total, there are eight formula units per elementary cell. In this structure, neither the V(V) nor the Mn(II) atom can be precisely assigned to a defined position. The atoms are statistically distributed in the Keggin framework. Thus, one in twelve of the twelve metal atoms is a V(V) or a Mn(II). The residual electron density of hydration water molecules, which could not be modeled due to high degree of disorder, was treated with a solvent mask function.

The powder XRD diffractograms of the individual substances and HPA-0-0 are shown in the Supporting Information in Figures S52–S58. The diffractograms differ from HPA-0-0 (Figure S52) and from each other, indicating successful incorporation of the metals. In general, the diffractograms show many reflexes, especially many reflexes with low intensity. This is an indicator that the powder contains different crystallographic phases of the same compound, which differ for example in their crystal water amount. The single crystals that were analyzed in this work on the other hand, consist of only one defined crystallographic phase. Different crystallographic phases can only be analyzed in the solid state via powder XRD, because the crystallographic phases are a phenomenon of the solid state and do not exist in solution.

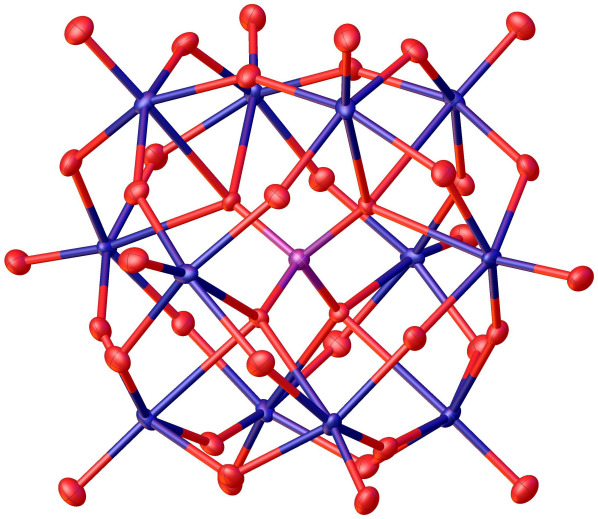

Figure 6. Structure of HPA-1-1 in the solid state as determined by x-ray diffraction, hydrogen atoms have not been modeled. The compound crystallized in space group Fd-3 m (227). There are six atoms in the asymmetric unit and eight formula units per elementary cell. Residual electron density attributed to hydration water has been refined with a solvent mask (aka SQUEEZE). R_1: 2.65, wR_2: 6.03 %, R_{int}: 2.78 %, GooF: 1.213. Purple: phosphorous, red: oxygen, and blue: metals (Mo, V, Mn).

The characteristics of the POMs in solution were investigated by ^{31}P- and ^{51}V NMR spectroscopy(Figure 7, Figure 8,

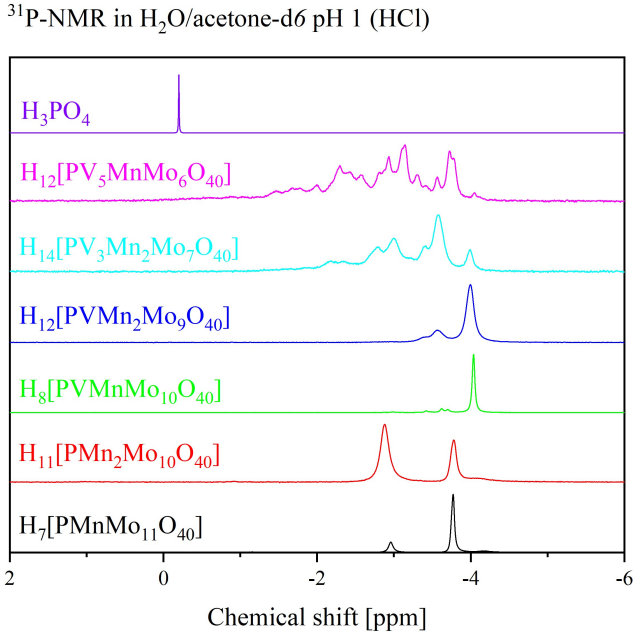

Figure 7. ^{31}P NMR spectra of the HPA-X-Y POMs in a mixture of 90 % H_2O (pH 1) and 10 % acetone-d6. The spectra were measured at 242.9 MHz. 85 % H_3PO_4 was used as external standard.

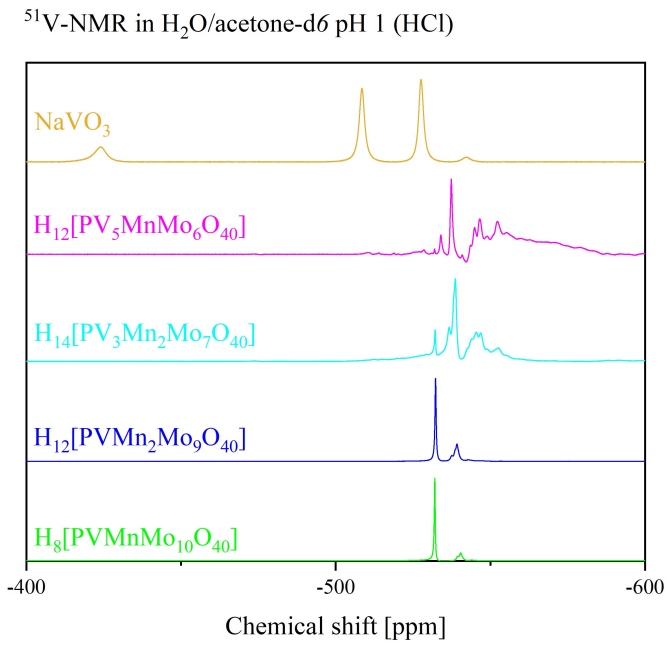

Figure 8. ^{51}V NMR spectra of the HPA–X-Y POMs in a mixture of 90% H_2O (pH 1) and 10% acetone-d6. The spectra were measured at 157.8 MHz. $NaVO_3$ was used as external standard.

and Figure 9) Although, in an unsubstituted structure like HPA-0-0, all metal centers are equivalent, the substitution of two or more metals leads to multiple possible isomers.[10,36–40] This is also observed in the ^{31}P NMR spectra of the newly discovered POMs, which exhibit several signals in the range of −2 ppm to -5 ppm. In particular, from the ^{31}P NMR spectra, the paramagnetism of Mn(II) is evident from broadening of the peaks. To visualize this, the ^{31}P NMR spectra of the two metal substituted POMs HPA-0-2 and HPA-1-1 were plotted in Figure 9 along with the ^{31}P NMR spectrum of HPA-0-0 which were all measured with the same parameters. The broadening of the peaks suggest the presence of the paramagnetic Mn(II) species.

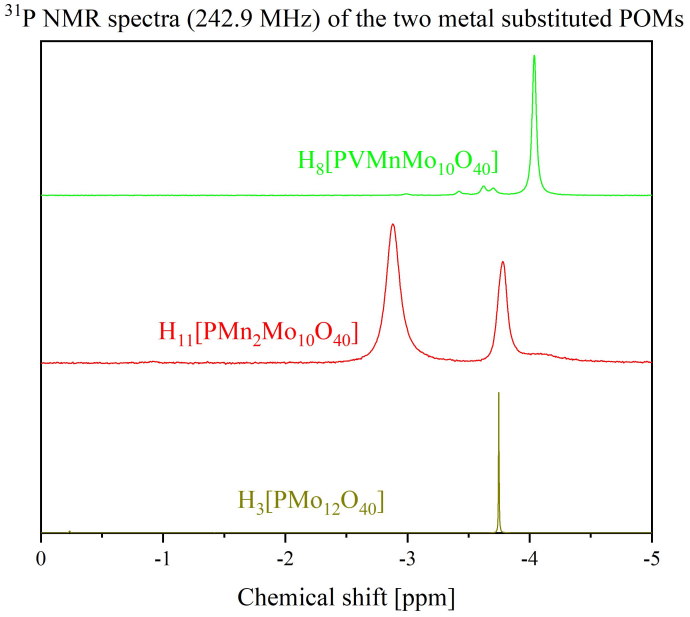

Figure 9. Comparison of the ^{31}P NMR spectra of the two metal substituted POMs HPA-0-2 and HPA-1-1 in comparison with HPA-0-0. The spectra indicate paramagnetism due to the broadening of the peaks in comparison to HPA-0-0.

^{51}V NMR spectroscopy can be used to verify the oxidation state of diamagnetic V(V). V(V) in the d^0-configuration is a diamagnetic species, while the reduced species, V(IV), with a d^1-configuration is a paramagnetic species that eludes observation by ^{51}V NMR spectroscopy.[43] The ^{51}V NMR spectra of the POMs (Figure 8) show several peaks in the range of −530 ppm to −560 ppm. The different ^{31}P- and ^{51}V-signals indicate a coexistence of the various isomers.[41,42] So the different peaks are attributed to the different positional isomers. It is also possible that two or more positional isomers have the same chemical shift and overlap in the spectra. Furthermore, it is also known that higher substituted POMs, especially those containing much V(V), dissociate in aqueous solution to lower or higher substituted POMs according to 2 $[PM_xV_y] \rightarrow [PM_{x+1}V_{y-1}] + [PM_{x-1}V_{y+1}]$.[39] This was studied for HPA-5 by Evtuguin et al.[39] It is also known that V(V) containing POMs set in aqueous solution one or more VO_2^+ cation free according to $[PM_xV_y] \rightarrow [PM_xV_{y-n}] + n\ VO_2^+$. The free VO_2^+ cations can be observed at -545 ppm in the ^{51}V spectra when they are present.[39]

For the only V(V) substituted Keggin-type POMs HPA-*X*-0 the following trend is observed: For HPA-1-0 ($X = 1$) all positions in the Keggin framework are equivalent, thus only one signal is observed in the ^{31}P- and ^{51}V NMR spectra, respectively. For HPA-2-0 there are 5, for HPA-3-0 13 and for HPA-6-0 there are even 48 positional isomers, so that 5, 13 and 48 signals can be detected in the respective spectra.[36] Since the chemical shifts of the various position isomers differ only slightly, especially in the case of the more highly V(V) substituted POMs, the signals in the NMR spectra often overlap.[10,36,39] Table 5 shows an overview of the chemical shifts obtained from ^{31}P- and ^{51}V NMR data (Figures 7 to 9) of the HPA-*X*-*Y* compounds in comparison with the ^{31}P NMR shifts of HPA-0-0.[10]

For future catalytic applications, the HOMO-LUMO (HOMO = highest occupied molecular orbital, LUMO = lowest unoccupied molecular orbital) gap and the redox potentials of the new POMs are of great interest. In order to further investigate the former measurements, UV/Vis spectra were measured (Figure 10). Since the scaffolding metal of a POM is generally present in its highest oxidation state, the HOMO-LUMO excitation is usually a Ligand-to-Metal-Charge-Transfer (LMCT) transition.[43–49] HPA-0-0 does not contain another foreign metal atom, therefore only the O→Mo(VI)O_6 LMCT at 218 nm is visible in the UV/Vis spectrum (Table 6, Supporting Information).[44–46] The HOMO of the POMs is mainly localized on the terminal oxygen atoms (M=O_t), so that its energetic position is not particularly affected by changes in the HPA framework. In contrast, the LUMO is more strongly influenced because the LUMO is localized on the d-orbitals of the framework metals and the bridging oxygen atoms (M–O–M). Changes in absorp-

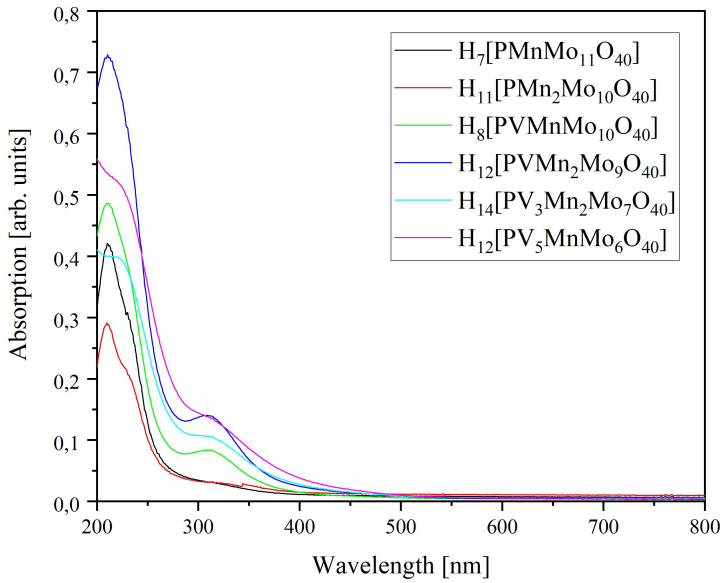

Figure 10. UV/Vis spectra of all HPA–X-Y compounds in water.

Table 6. LMCT peaks from al HPA–X-Y compounds in water.

LMCT	HPA-0-0	HPA-0-1	HPA-0-2	HPA-1-1	HPA-1-2	HPA-3-2	HPA-5-1
$O\rightarrow Mo(VI)O_6$	218	211	210	210	211	215	214
$O\rightarrow V(V)O_6$	–	–	–	311	309	305	310

tion therefore mainly reflect changes in the energetic position of the LUMO.[44]

For V(V)-substituted POMs, two LMCT transitions are possible: ligand to Mo(VI) and ligand to V(V) (Table 6, Supporting Information). The incorporation of Mn(II) is not expected to add an additional transition, as Mn(II) is known for its d^5-high spin configuration in which the transition between the metals d-orbitals are forbidden and there is no room for an LMCT excitation (see Figure S60 Supporting Information).[43]

The spectra shown in Figure 10 exhibit maxima between 210 nm and 218 nm, which correspond to the LMCT excitation from oxygen to Mo(VI). The broad and less intense bands between 305 nm and 311 nm correspond to the LMCT transitions of oxygen to V(V) (Table 6). The LMCT bands of the V(V) are very broad and extend into the visible range. This is what gives rise to the different colors of the HPA-*X*-Y compounds. Since the HPA-0-1 does not contain V(V) and Mn(II) does not have a LMCT, this POM appears yellow, just like the parent POM HPA-0-0. As the amount of V(V) increases, the O→V(V) LMCT appears in the visible region, so the HPA-1-1 has a red color. With increasing amounts of V(V), the intensity of the V(V) LMCT increases accordingly, while the intensity of the Mo(VI) LMCT decreases proportionally. This results in a brown color dominating the POMs when more V(V) is incorporated into the Keggin structure.[47] Figure 11 shows all HPA-*X*-*Y* POMs with their different colors sorted by degree of substitution.

In comparison with the LMCT bands of the HPA-*X*-0 POMs (Table 6 in the Supporting Information), it is noticeable that the LMCT bands for Mo(VI) are in the range between 213 nm and 219 nm, while the LMCT bands for V(V) are in the range between 302 nm and 320 nm. This does not represent a significant difference to the HPA-*X*-*Y* POMs, so that it can be assumed that Mn(II) does not influence the position of the LMCT bands for Mo(VI) and V(V) strongly enough. However, it is already known for the HPA-*X*-0 compounds that the LMCT band for V(V) has a shoulder in the direction of longer wavelength. The band for the V(V) LMCT at smaller wavelength can be assigned to the $V{=}O_t$ band (transition of an electron from the orbitals of the terminal oxygen atoms into the acceptor orbitals of the V(V) atoms) and the band causing the shoulder at larger wavelength can be assigned to the $V\text{-}O_b$/$V\text{-}O_c$ bonds (transition of an electron from the orbitals of the metal-bridging oxygen atoms into the acceptor orbitals of the V(V) atoms).[47,50] Similar trends have already been observed in the LMCT for Mo(VI).[51] It is also known for the HPA-*X*-0 POMs that a red shift of the LMCT bands occurs with decreasing pH value.[47,51]

Furthermore, the UV/Vis spectroscopy results compiled here can be used to indirectly infer the oxidation states of the elements involved: no LMCT can be expected for Mn(II) in the d^5-high spin configuration because the transitions are forbidden. Mo(VI) and V(V) are in their respective highest oxidation states (d^0-configuration). Reduced species of the elements Mo and V would not correspond to the d^0-configuration, so that the transitions are forbidden and no LMCT can be observed.[43]

Since the goal of our synthesis was to tune the POMs redox activity, electrochemical measurements were performed.[52–58]

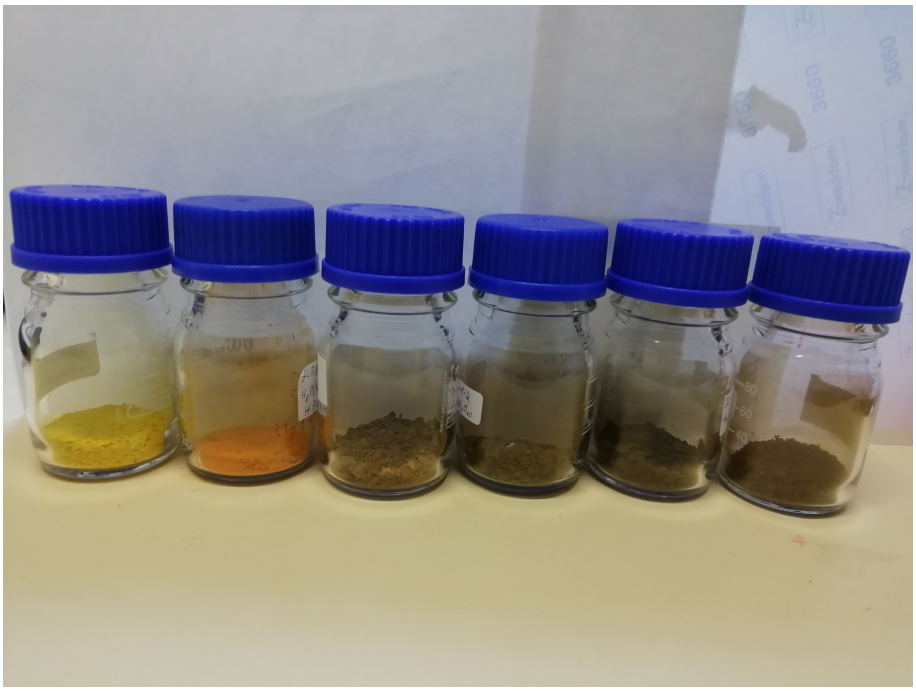

Figure 11. HPA-X-Y POMs synthesized in this work with their different colors. From left to the right: HPA-0-1, HPA-1-1, HPA-0-2, HPA-1-2, HPA-3-2, HPA-5-1.

The redox potentials of the new synthesized POMs were measured with cyclic voltammetry (CV) and square wave voltammetry (SWV). A comparison of the data from the two-fold substituted POMs is shown in Figure 12 (CV) and 13 (SWV), the remaining CV and SWV data of the individual POMs can be found in the Supporting Information (Figure S61 und S62), respectively. The data of the two-fold substituted POMs in Figure 12 and 13 are compared with the two-fold only V(V) substituted POM HPA-2-0 and with the unsubstituted POM HPA-0-0 to get and better overview.

The CV/SWV curves of the two metal V(V) containing POMs, HPA-1-1 and HPA-2-0 are very similar, whereas the CV/SWV

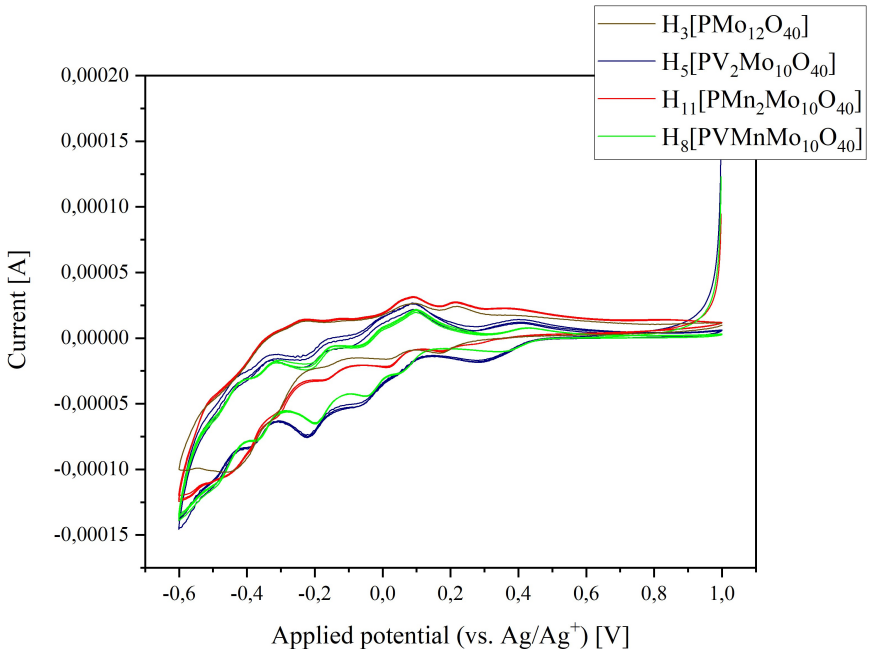

Figure 12. Comparison between the CV measurements of the two-fold metal substituted POMs HPA-2-0, HPA-0-2, HPA-1-1 and HPA-0-0 (concentration 1 mmol/L, scan rate 100 mV/s (CV)/5 mV/s (SWV) and pH 1).

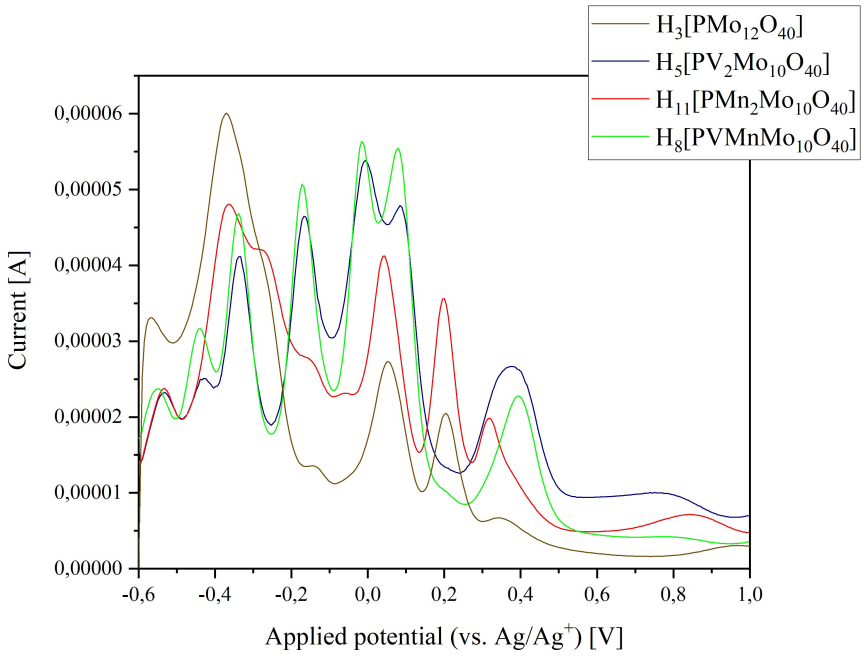

Figure 13. Comparison between the SWV measurements of the two-fold metal substituted POMs HPA-2-0, HPA-0-2, HPA-1-1 and HPA-0-0 (concentration 1 mmol/L, scan rate 100 mV/s (CV)/5 mV/s (SWV) and pH 1).

curve of the purely Mn(II) substituted HPA-0-2 deviates significantly. This leads to the conclusion that Mn(II) is present and takes part in the redox processes. In the SWV measurements, the V(V) containing two-fold substituted POMs both exhibit a pattern of two overlapping peaks in the range between −100 mV and 200 mV. In contrast, HPA-0-0 and HPA-0-2 do not show this pattern, indicating that these peaks are caused by the redox activity of V(V). HPA-0-0 and HPA-0-2 show only peaks at 50 mV (HPA-0-0) and 44.6 mV (HPA-0-2), respectively. These peaks can therefore only originate from redox processes of Mo(VI). Apparently, the Mn(II) incorporation leads to a shift of the redox processes from Mo(VI) to lower potentials.

The solely Mn(II) containing Keggin-type POMs HPA-0-2 shows three nearly overlapping peaks in the range between −400 and −100 mV, a feature not seen in the other V(V) containing POMs. The peak of HPA-0-2 at 201 mV is also not seen in the other V(V) substituted POMs, but for HPA-0-0 at 205 mV. Apparently, the peak of HPA-0-2 at 316 mV shifts through 377 mV for HPA-2-0 to 392 mV for HPA-1-1. For HPA-0-0, however, this peak is very weak at 340 mV.

The more V(V) the POMs contain, the more the signals merge in the range between −200 mV and 200 mV. This trend is particularly evident for the POMs HPA-3-2 and HPA-5-1 with three and five V(V) atoms in the structure (see CV and SWV data in the Supporting Information in Figures S30, S36 and S62). A table showing the peak maxima in all the SVW data and the maxima and minima in all the CV data is included in the Supporting Information (Table 7). The plot of the CV/SWV data of the POMs with three and five V(V) atoms in Figure S62 also contain the CV/SWV data of HPA-0-0, HPA-2-0 and HPA-0-2 to emphasize the differences to these compounds.

The electrochemical measurements of the triple and quintuple V(V) substituted POMs (Figure S62 Supporting Information) show significant differences from the low V(V) substituted POMs, while the Mn(II) substituted POMs show less significant differences. This can be explained by the fact that a maximum of six out of twelve Mo(VI) positions in the Keggin framework can be substituted by V(V), while only a maximum of two of the twelve positions can be occupied by Mn(II). The more metal atoms of the same species are integrated into the Keggin structure, the more significant its effects become, which

Table 7. Selected two-electron processes observed for the different HPA-0-Y species in comparison with HPA-0-0.

POM	Process	Peak maxima SWV [mV]
HPA-0-0	$[PMo^{VI}_{11}Mo^{IV}O_{40}]^{5-}/[PMo^{VI}_{12}O_{40}]^{3-}$	50
	$[PMo^{VI}_{10}Mo^{IV}_{2}O_{40}]^{7-}/[PMo^{VI}_{11}Mo^{IV}O_{40}]^{5-}$	205
HPA-0-1	$[PMnMo^{VI}_{10}Mo^{IV}O_{40}]^{9-}/[PMnMo^{VI}_{11}O_{40}]^{7-}$	39.5
	$[PMnMo^{VI}_{9}Mo^{IV}_{2}O_{40}]^{11-}/[PMnMo^{VI}_{10}Mo^{IV}O_{40}]^{9-}$	201
HPA-0-2	$[PMn_2Mo^{VI}_{9}Mo^{IV}O_{40}]^{13-}/[PMn_2Mo^{VI}_{10}O_{40}]^{11-}$	46.6
	$[PMn_2Mo^{VI}_{8}Mo^{IV}_{2}O_{40}]^{15-}/[PMn_2Mo^{VI}_{9}Mo^{IV}O_{40}]^{13-}$	201

Table 8. Shift of the RedOx potential V(V)→V(IV) depending on the substitution with V(V) and Mn(II).

POM	HPA-2-0	HPA-1-1	HPA-1-2
Redox potential V(V)→V(IV) [mV]	84.8	79.8	74.8

is also reflected in the SWV plot of $H_{11}PMn_2Mo_{10}O_{40}$ for two Mn(II) atoms in the structure.

From the literature it is known that HPA-0 (Figure S61 in the Supporting Information) has two significant two-electron processes (1: CV: 8.33 mV/87.7 mV; SWV: 50 mV and 2: CV: 167 mV/218 mV; SWV: 205 mV) resulting from $[PMo^{VI}_{11}Mo^{IV}O_{40}]^{5-}$/$[PMo^{VI}_{12}O_{40}]^{3-}$ and $[PMo^{VI}_{10}Mo^{IV}_{2}O_{40}]^{7-}$/$[PMo^{VI}_{11}Mo^{IV}O_{40}]^{5-}$.[59,60] These processes are also found for the other POMs and are listed in Table 7:

The listed potentials become lower than in HPA-0-0 when Mn(II) is present for HPA-0-1 and HPA-0-2. This shows the trend that Mn(II) lowers the potentials for the different redox processes of a POM. For the higher substituted POMs these processes are not observed anymore, because of the overlapping redox processes of V(V). It is also possible, that anions with metals in different oxidations states and an overall charge greater than −12, are not stable enough to form.

The peak at 84.8 mV (HPA-2-0), 79.8 mV (HPA-1-1) and 74.8 mV (HPA-1-2) belongs to the redox process of V(V)→V(IV) in the VO_2^+ ion (Table 8), which is formed via dissociation of the HPA-*X*-*Y* POMs in solution (HPA-*X*-*Y*→VO_2^+ + HPA-(*X*-1)-*Y*).[58] Vanadium is responsible for the catalytic redox activity: in the first step the reduction (V(V)→V(IV)) occurs, so that the substrate is oxidized. After this step the catalyst can be oxidized again (V(IV)→V(V)), e.g. with molecular oxygen.[58] Our measurements show that the corresponding potentials are lowered by the introduction of Mn(II), thereby indicating that we have successfully tuned the redox potential.

Conclusion

A synthetic procedure that allows the substitution of the scaffolding metal of Keggin-type POMs with Mn(II) and V(V) was developed. Using this procedure, it was possible to synthesize and isolate several bi- and trimetallic Keggin-type-POMs. The composition and structure were confirmed by ICP-OES and vibrational spectroscopy. Furthermore, the new compounds were comprehensively characterized with NMR spectroscopy, UV/Vis spectroscopy, electrochemical methods and single crystal X-ray diffraction. We were able to show that the introduction of Mn(II) lowered the electrochemical potential of the V(V)/V(IV) RedOx process, which is a promising step towards tunable RedOx properties. Overall, our analytical results provide a solid basis for future investigations on the catalytic activity of Mn(II), and Mn(II)/V(V)-substituted phosphomolybdates.

Experimental Section

The following synthetic procedure was adapted from Odyakov and Zhizhina.[9,16] Detailed synthetic procedures for each compound can be found in the Supporting Information.

For the synthesis of HPA-*X*-*Y* two separate solutions were prepared:

Solution 1: Divanadium pentoxide was added to deionized water and cooled to 5 °C. Then a 30% hydrogen peroxide solution in water was added dropwise to the orange-coloured suspension and stirred for some time, whereupon a brown solution was formed from which oxygen gas evolution was observed. The solution was then warmed to room temperature and a 25% phosphoric acid solution in water was added and the solution was cooled to 5 °C again.

Solution 2: Molybdenum trioxide was suspended in deionized water and a 25% phosphoric acid solution in water was added. Then the suspension was heated to reflux, whereupon a yellow, clear solution formed after about one hour.

The cool solution 1 was added dropwise to the boiling solution 2 and further heated to reflux. After 30 min, a manganese(II) acetate solution in water was added to the dark-coloured solution and heated to reflux for a further 90 min. The solution was then cooled to room temperature, filtered and concentrated under reduced pressure and elevated temperature (rotary evaporator with oil bath at 85 °C and 400 to 0 mbar).

The vanadium-free, manganese(II)-substituted POMs were synthesized according to the following modified prescription:

Deionized water was introduced, molybdenum trioxide and a 25% phosphoric acid solution in water were added and heated to reflux. After one hour, a yellow, clear solution was formed. Subsequently, a solution of manganese(II) acetate in water was added to the boiling solution and heated to reflux for another 60 minutes after the addition was completed. The solution was cooled to room temperature, filtered and concentrated under reduced pressure (rotary evaporator with oil bath at 85 °C and 400 to 0 mbar).

Further experimental details are provided in the Supporting Information.

Deposition Number(s) 2141261 (for HPA-0-1), 2141263 (for HPA-0-2), 2141259 (for HPA-1-1), 2141262 (for HPA-1-2), 2141260 (for HPA-5-1) contain(s) the supplementary crystallographic data for this paper. These data are provided free of charge by the joint Cambridge Crystallographic Data Centre and Fachinformationszentrum Karlsruhe Access Structures service.

Acknowledgements

The authors thank the central x-ray facility of Hamburg University, especially Dr. Frank Hoffmann for his help in solving and refining the structures and Isabelle Nevoigt for data collection. Furthermore, the authors gratefully acknowledge Prof. Irina Smirnova for allowing the use of her TGA machine at the Hamburg University of Technology. We further thank in particular Thomas Marx from the research group of Prof. Dr. Peter Burger for providing electrochemical equipment and helping with the electrochemical measurements. Open Access funding enabled and organized by Projekt DEAL.

Conflict of Interest

The authors declare no conflict of interest.

Keywords: crystallography · electrochemistry · polyoxometalates · redox active elements · NMR spectroscopy

[1] N. I. Gumerova, A. Rompel, *Nat. Chem. Rev.* **2018**, *2*, 1–20.
[2] F. Lu, M. Wang, N. Li, B. Tang, *Chem. Eur. J.* **2021**, *27*, 6422–6434.
[3] L. Yang, J. Lei, J. M. Fan, R. M. Yuan, M. Sen Zheng, J. J. Chen, Q. F. Dong, *Adv. Mater.* **2021**, *33*, 1–25.
[4] Y. F. Song, R. Tsunashima, *Chem. Soc. Rev.* **2012**, *41*, 7384–7402.
[5] R. Neumann, *Inorg. Chem.* **2010**, *49*, 3594–3601.
[6] J. Reichert, B. Brunner, A. Jess, P. Wasserscheid, J. Albert, *Energy Environ. Sci.* **2015**, *8*, 2985–2990.
[7] B. Bertleff, J. Claußnitzer, W. Korth, P. Wasserscheid, A. Jess, J. Albert, *ACS Sustainable Chem. Eng.* **2017**, *5*, 4110–4118.
[8] K. Inumaru, T. Ishihara, Y. Kamiya, T. Okuhara, S. Yamanaka, *Angew. Chem. Int. Ed.* **2007**, *46*, 7625–7628; *Angew. Chem.* **2007**, *119*, 7769–7772.
[9] V. F. Odyakov, E. G. Zhizhina, *React. Kinet. Catal. Lett.* **2008**, *95*, 21–28.
[10] J. Albert, D. Lüders, A. Bösmann, D. M. Guldi, P. Wasserscheid, *Green Chem.* **2014**, *16*, 226–237.
[11] M. Abbessi, R. Contant, R. Thouvenot, G. Hervé, *Inorg. Chem.* **1991**, *30*, 1695–1702.
[12] A. Patel, N. Narkhede, S. Singh, S. Pathan, *Catal. Rev. Sci. Eng.* **2016**, *58*, 337–370.
[13] M. T. Pope, A. Müller, *Polyoxometalate Chemistry From Topology via Self-Assembly to Applications*, New York, Boston, Dordrecht, London, Moscow, **2002**.
[14] A. Gaspar, D. V. Evtuguin, C. P. Neto, *Holzforschung* **2004**, *58*, 640–649.
[15] A. Patel, S. Pathan, *J. Coord. Chem.* **2012**, *65*, 3122–3132.
[16] V. F. Odyakov, E. G. Zhizhina, *Russ. J. Inorg. Chem.* **2009**, *54*, 361–367.
[17] F. Zhang, M. Guo, H. Ge, J. Wang, *Front. Chem. Eng. China* **2007**, *1*, 296–299.
[18] V. F. Odyakov, E. G. Zhizhina, R. I. Maksimovskaya, *Appl. Catal. A* **2008**, *342*, 126–130.
[19] A. J. Bridgeman, *Chem. Eur. J.* **2004**, *10*, 2935–2941.
[20] J. K. Lee, J. Melsheimer, S. Berndt, G. Mestl, R. Schlögl, K. Köhler, *Appl. Catal. A* **2001**, *214*, 125–148.
[21] G. Mestl, T. Ilkenhans, D. Spielbauer, M. Dieterle, O. Timpe, J. Kröhnert, F. Jentoft, H. Knözinger, R. Schlögl, *Appl. Catal. A* **2001**, *210*, 13–34.
[22] O. V. Dolomanov, L. J. Bourhis, R. J. Gildea, J. A. K. Howard, H. Puschmann, *J. Appl. Crystallogr.* **2009**, *42*, 339–341.
[23] C. B. Hübschle, G. M. Sheldrick, B. Dittrich, *J. Appl. Crystallogr.* **2011**, *44*, 1281–1284.
[24] A. L. Spek, *J. Appl. Crystallogr.* **2003**, *36*, 7–13.
[25] G. M. Sheldrick, *Acta Crystallogr. Sect. A* **2008**, *64*, 112–122.
[26] A. L. Spek, *Acta Crystallogr. Sect. D* **2009**, *65*, 148–155.
[27] A. L. Spek, *Acta Crystallogr. Sect. C* **2015**, *71*, 9–18.
[28] H. H. Wu, Z. M. Zhang, E. B. Wang, *Chin. Chem. Lett.* **2012**, *23*, 355–358.
[29] H.-X. Liu, Q. Liu, L.-T. Wang, Q.-H. Fan, K.-Q. Ye, G. Zeng, X.-S. Tai, *Asian J. Chem.* **2014**, *26*, 4741–4743.
[30] P. Pyykkö, M. Atsumi, *Chem. Eur. J.* **2009**, *15*, 186–197.
[31] M. X. Xu, S. Lin, L. M. Xu, S. L. Zhen, *Transition Met. Chem.* **2004**, *29*, 332–335.
[32] P. Kubácek, R. Hoffmann, *J. Am. Chem. Soc.* **1981**, *103*, 4320–4332.
[33] M. Darari, A. Francés-Monerris, B. Marekha, A. Doudouh, E. Wenger, A. Monari, S. Haacke, P. C. Gros, *Molecules* **2020**, *25*, 5991–6011.
[34] C. K. H. Borg, X. Zhou, C. Eckberg, D. J. Campbell, S. R. Saha, J. Paglione, E. E. Rodriguez, *Phys. Rev. B* **2016**, *93*, 1–10.
[35] J. Li, A. W. Sleight, *J. Solid State Chem.* **2004**, *177*, 889–894.
[36] M. T. Pope, T. F. Scully, *Inorg. Chem.* **1975**, *14*, 953–954.
[37] L. Pettersson, I. Andersson, A. Selling, J. H. Grate, *Inorg. Chem.* **1994**, *33*, 982–993.
[38] A. Selling, I. Andersson, J. H. Grate, L. Pettersson, *Eur. J. Inorg. Chem.* **2000**, 1509–1521.
[39] D. V. Evtuguin, C. Pascoal Neto, J. Rocha, J. D. Pedrosa De Jesus, *Appl. Catal. A* **1998**, *167*, 123–139.
[40] K. Lee, G. Pozarnsky, O. Zarembowitch, A. McCormick, *Chem. Eng. J. Biochem. Eng. J.* **1996**, *64*, 215–223.
[41] J. Albert, M. Mendt, M. Mozer, D. Voß, *Appl. Catal. A* **2019**, *570*, 262–270.
[42] S. Wesinger, M. Mendt, J. Albert, *ChemCatChem* **2021**, *13*, 3662–3670.
[43] A. F. Holleman, E. Wiberg, Nils Wiberg, G. Fischer, *Lehrbuch Der Anorganischen Chemie*, Berlin, New York, **2009**.
[44] K. P. Barteau, J. E. Lyons, I. K. Song, M. A. Barteau, *Top. Catal.* **2006**, *41*, 55–62.
[45] I. K. Song, H. S. Kim, M. S. Chun, *Korean J. Chem. Eng.* **2003**, *20*, 844–849.
[46] T. Yamase, *Chem. Rev.* **1998**, *98*, 307–325.
[47] J. Claußnitzer, *Oxidative Entschwefelung von Mineralökfraktionen Mit Vanadiumhaltigen Polyoxometallat-Katalysatoren*, Bayreuth, **2021**.
[48] H. Salavati, N. Rasouli, *Mater. Res. Bull.* **2011**, *46*, 1853–1859.
[49] H. Li, L. Swenson, R. J. Doedens, M. I. Khan, *Dalton Trans.* **2016**, *45*, 16511–16518.
[50] N. K. K. Raj, A. V. Ramaswamy, P. Manikandan, *J. Mol. Catal. A* **2005**, *227*, 37–45.
[51] Q. Gao, F. Li, M. Sun, L. Xu, Y. Wang, J. Bai, *CrystEngComm* **2014**, *16*, 7681–7688.
[52] N. Elgrishi, K. J. Rountree, B. D. McCarthy, E. S. Rountree, T. T. Eisenhart, J. L. Dempsey, *J. Chem. Educ.* **2018**, *95*, 197–206.
[53] M. Privman, T. Hepel, *J. Electroanal. Chem.* **1995**, *382*, 137–144.
[54] C. Li, Y. Zhang, K. P. O'Halloran, J. Zhang, H. Ma, *J. Appl. Electrochem.* **2009**, *39*, 421–427.
[55] M. Barth, M. Lapkowski, S. Lefrant, *Electrochim. Acta* **1999**, *44*, 2117–2123.
[56] T. Ueda, *ChemElectroChem* **2018**, *5*, 823–838.
[57] Z. Han, Y. Zhao, J. Peng, Y. Feng, J. Yin, Q. Liu, *Electroanalysis* **2005**, *17*, 1097–1102.
[58] B. Bujanovic, S. Ralph, R. Reiner, K. Hirth, R. Atalla, *Materials* **2010**, *3*, 1888–1903.
[59] D. Youn Hwang, S. Yong Ha, S. Kim, *Bull. Korean Chem. Soc.* **2001**, *22*, 441–442.
[60] M. Sadakane, E. Steckhan, *Chem. Rev.* **1998**, *98*, 219–237.

Manuscript received: April 11, 2022
Accepted manuscript online: June 22, 2022
Version of record online: July 13, 2022